Neurexins control the strength and precise timing of glycinergic inhibition in the auditory brainstem

He-Hai Jiang[1,2,3], Ruoxuan Xu[1], Xiupeng Nie[1], Zhenghui Su[1], Xiaoshan Xu[1], Ruiqi Pang[4,5], Yi Zhou[4], Fujun Luo[1,2,3]*

1. Guangzhou National Laboratory, 510005, Guangzhou, Guangdong, China
2. Bioland Laboratory, 510005, Guangzhou, Guangdong, China
3. School of Basic Medical Sciences, Guangzhou Medical University, 510005, Guangzhou, Guangdong, China
4. Department of Neurobiology, School of Basic Medicine, Army Medical University, 400038, Chongqing, China
5. Advanced Institute for Brain and Intelligence, School of Medicine, Guangxi University, 530004, Nanning, China

*Correspondence author. luo_fujun@gzlab.ac.cn (F.L.)

Abstract

Neurexins play diverse functions as presynaptic organizers in various glutamatergic and GABAergic synapses. However, it remains unknown whether and how neurexins are involved in shaping functional properties of the glycinergic synapses, which mediate prominent inhibition in the brainstem and spinal cord. To address these issues, we examined the role of neurexins in a model glycinergic synapse between the principal neuron in the medial nucleus of the trapezoid body (MNTB) and the principal neuron in the lateral superior olive (LSO) in the auditory brainstem. Combining RNAscope with stereotactic injection of AAV-Cre in the MNTB of neurexin1/2/3 conditional triple knockout mice, we showed that MNTB neurons highly express all isoforms of neurexins although their expression levels vary remarkably. Selective ablation of all neurexins in MNTB neurons reduced not only the amplitude but also the kinetics of the glycinergic synaptic transmission at LSO neurons. The synaptic dysfunctions were primarily caused by impaired Ca^{2+} sensitivity of release and tightness of coupling between voltage-gated Ca^{2+} channels and synaptic vesicles. Together, our current findings demonstrate that neurexins are essential in controlling the strength and temporal precision of the glycinergic synapse, which therefore corroborates the role of neurexins as key presynaptic organizers in all major types of fast chemical synapses.

Introduction

Neurexins are evolutionarily conserved synaptic adhesion molecules and their genetic mutations are highly associated with autism and schizophrenia (Gomez et al., 2021; Sudhof, 2008; 2017). In the vertebrate, neurexins are encoded by three genes Nrxn1, Nrxn2, Nrxn3, each of which contains distinct promoters for expressing longer α- and shorter β-neurexins (Ullrich et al., 1995; Ushkaryov et al., 1992). Both α- and β-neurexins are critical and non-redundant in regulating the formation and function of synapses (Anderson et al., 2015; Missler et al., 2003; Sudhof, 2017). Triple knockout (KO) of α-neurexins causes a significant decrease in the density of GABAergic but not glutamatergic synapses while producing a strong reduction in both inhibitory and excitatory synaptic transmission(Missler *et al.*, 2003). Triple KO of β-neurexins reveals a significant phenotype only in glutamatergic synapses, but not in GABAergic synapses (Anderson *et al.*, 2015). Deletion of all neurexins, including Nrxn1/2/3 α- and β-neurexins, leads to profound but strikingly distinct phenotypes in different synapses, which further supports diverse actions of neurexins in specific neurons (Chen et al., 2017; Luo et al., 2020). Consistently, transcriptomic analysis has revealed that the expression profiles of various neurexins differ remarkably in excitatory neurons versus inhibitory neurons even among distinct subtypes of interneurons (Foldy et al., 2016; Fuccillo et al., 2015; Lukacsovich et al., 2019; Uchigashima et al., 2019). Despite the multifaceted roles of neurexins widely observed in various glutamatergic and GABAergic synapses (Boxer and Aoto, 2022; Chen *et al.*, 2017; Luo et al., 2021; Sudhof, 2017), however, it remains largely unknown how neurexins may regulate the functional properties of the glycinergic synapses, which mediate essential inhibition in the spinal cord, brainstem and retina (Assareh et al., 2023; Brill et al., 2020; Chang et al., 2023; Feng et al., 1998; Foster et al., 2015; Gomeza et al., 2003a; Gomeza et al., 2003b; Zeilhofer et al., 2012).

In the mammalian auditory brainstem, it is well-characterized that the principal neurons in the medial nucleus of the trapezoid body (MNTB) project glycinergic synaptic inputs to the lateral superior olive (LSO) (Fischer et al., 2019; Kotak et al., 1998; Nabekura et al., 2004; Sanes and Friauf, 2000). These synapses are robust, precise and extremely reliable even during high frequency stimulation(Krachan et al., 2017). Strong evidence has shown that the

MNTB-LSO glycinergic synapses are subject to extensive refinement during development, including transmitter type switch, the elaboration of dendrites and axonal arbors followed by synaptic pruning, to achieve exquisite control of fast inhibition(Brill *et al.*, 2020; Kim and Kandler, 2003; Kotak *et al.*, 1998; Nabekura *et al.*, 2004; Sanes and Friauf, 2000). However, the molecular mechanisms of shaping their functional characteristic remain incompletely understood.

We utilized the triple Nrxn1/2/3 conditional KO mice (Nrxn123 cTKO) (Chen *et al.*, 2017) to ablate all neurexins in MNTB principal neurons with stereotactic injection of associated adeno-virus (AAV) expressing Cre-recombinase. Combined with RNAscope technique, we verified that MNTB neurons highly express various isoforms of neurexins. Selective injection of AAV-Cre, but not AAV-EGFP, successfully blocked expression of all neurexins in MNTB neurons. Functionally, pan-neurexin deletion significantly impaired both the amplitude and the kinetics of the glycinergic synaptic transmission. Surprisingly, deletion of all neurexins led to a significantly higher number of glycinergic synapses innervating the LSO and higher frequency of spontaneous neurotransmitter release. Application of low extracellular Ca^{2+} blocked the glycinergic neurotransmission of both control and neurexin-deficient synapses, but with a significant difference in its effectiveness. Moreover, treatment with EGTA, a high-affinity Ca^{2+} chelator with slow binding kinetics, caused a much stronger inhibition of neurotransmission in neurexin-deficient synapses, suggesting a significant disruption of the tight coupling between voltage-gated Ca^{2+} channels and synaptic vesicles in the MNTB-LSO glycinergic synapses.

Results

Neurexins are highly expressed in MNTB neurons

To study the role and mechanism of neurexins in the glycinergic synapse between MNTB neurons and LSO neurons, which are critical in computing sound localization in mammalian auditory brainstem (Grothe et al., 2010), we first characterized the expression of Nrxn1-3 in the principal neurons of the MNTB by fluorescent *in-situ* hybridization (FISH) using RNAscope technique. As shown in Figure 1, MNTB neurons in wild-type (WT) mice expressed Nrxn1, Nrxn2, and Nrxn3, although the expression level of each gene appeared to vary remarkably.

As an initial exploration, we took advantage of Nrxn123 cTKO mice that enable deletion of all neurexins following the expression of Cre recombinase (Chen *et al.*, 2017), to bypass the functional redundancy of different neurexins. Neuronal specific deletion of all neurexins was achieved by stereotactic injection of AAV-Cre-EGFP into the MNTB at P0 (TKO). As control, AAV-EGFP was injected (Ctrl). Successful virus injection and expression of Cre recombinase in MNTB neurons were confirmed by strong EGFP fluorescence (Figure 1d-e). FISH data further demonstrated that the recombinase dramatically blocked the expression of all neurexins, as compared to the normal expression of neurexins when EGFP was expressed (Figure 1f, compared to 1b). Altogether, these data show that the glycinergic neurons in the MNTB highly express various neurexin genes, which can be specifically deleted by stereotactic injection of AAV-Cre in Nrxn123 cTKO mice.

Neurexins are essential for dictating the strength and kinetics of the MNTB-LSO glycinergic synapse

Since neurexins play an essential role in orchestrating functional organization of various synapses including both glutamatergic and GABAergic synapses, we hypothesize that deletion of all neurexins may have a significant impact on glycinergic synapses. To test the hypothesis, we sought to examine how neurexins may regulate the function of the MNTB-LSO glycinergic synapse in the auditory brainstem. Because LSO neurons receive excitatory glutamatergic inputs and inhibitory GABAergic/glycinergic inputs, we used a pharmacologic approach to isolate the glycinergic inputs. By blocking glutamatergic inputs with CNQX and AP5, we were able to selectively record inhibitory postsynaptic currents (IPSCs) from LSO neurons, which can be completely inhibited by strychnine, a potent glycine receptor inhibitor (Figure S1).

To specifically examine the role of neurexins in regulating the glycinergic synapse, we used an optogenetic approach in which two AAVs, AAV-Cre-EGFP and AAV-DIO-ChR2-mCherry, were co-injected in Nrxn123 cTKO mice. As control, AAV-ChR2-EYFP was used for injection. Virus injection was performed at P0 and acute slices derived from these mice were analyzed at P13-14. We verified the successful expression of ChR2 by examining the fluorescence and further by recording optogenetic-evoked action

potentials from the soma of MNTB neurons. Reliable action potential (AP) firing can be induced by single or repetitive high-frequency light stimulation (Figure S1c). In control mice, optogenetic stimulation of MNTB neurons robustly triggered large IPSCs recorded from LSO neurons (Figure 2a-b), which can be fully blocked by strychnine (Figure S1d) and are thus purely glycinergic. In TKO mice with co-injection of Cre and ChR2, however, optogenetic stimulation induced significantly smaller IPSCs (Figure 2a-b). On average, we observed ~60% reduction in the peak amplitude (Figure 2b), similar to previous findings at other different synapses (Chen *et al.*, 2017; Luo *et al.*, 2020). Furthermore, the kinetics of IPSCs were dramatically reduced as indicated by significantly slower rise time and decay time in TKO mice as compared to control (Figure 2c-d). Together, these data strongly suggest that neurexins are essential for the intact function of the glycinergic synapse.

To further address the physiological role of neurexins in action potential evoked neurotransmission at the glycinergic synapse, we applied electric stimulation to activate presynaptic fibers of MNTB neurons by placing a stimulating electrode in the midway between the MNTB and the LSO. Consistent with our optogenetic approach, afferent-evoked large IPSCs were predominantly glycinergic as they can also be fully blocked by strychnine (Figure S1). A modest but significant decrease in synaptic strength was observed in Nrxn123 TKO mice as compared to control mice (Figure 2e-f), confirming the important role of neurexins in the glycinergic synapses. The modest effect of the pan-neurexin deletion on synaptic strength in the MNTB-LSO synapses is likely due to the incomplete AAV virus transfection in MNTN neurons. Therefore, it is likely that a small fraction of MNTB neurons may still express relatively normal expression of neurexins. It is worth pointing out that extensive efforts were made to optimize our virus injection protocols by adjusting the injection parameters including the needle angle, virus titers, and volume. On average, it was estimated that approximately ~80% neurons in the MNTB expressed GFP and thus infected by AAV-Cre. It is also possible that other sources of glycinergic inputs other than the MNTB afferents are likely to present but obscured in wild-type animals by the predominant glycinergic inputs from MNTB neurons (Jalabi et al., 2013).

The mechanism of neurexins for regulating the MNTB-LSO glycinergic synapse

Since neurexins play multifaceted roles in regulating pre- and/or post-synaptic functions, we explored the potential mechanisms by initially examining the paired-pulse ratio (PPR) of IPSCs, which have been routinely used for identifying a presynaptic origin of regulation. As shown in Figure 2h, IPSCs evoked by two consecutive stimuli at various intervals showed a strong depression in both control and TKO mice. However, the PPRs were significantly increased by deletion of neurexins (Figure 2i), suggesting that neurexins are required for maintaining a high release probability of the glycinergic nerve terminal.

We then recorded and analyzed spontaneous IPSCs from LSO neurons. Compared to control, there was no significant difference in both the amplitude and kinetics of sIPSCs (Figure 3a-d) in TKO mice, indicating the normal content of synaptic vesicle as well as the normal function of postsynaptic glycine receptors. Surprisingly, however, we found that deletion of all neurexins caused a small but significant increase in the frequency of sIPSCs (Figure 3a-b), which is opposite to previous reports of either no change or decrease in the miniature frequency at glutamatergic or GABAergic synapse (Chen *et al.*, 2017; Luo *et al.*, 2020). To test whether the increase in sIPSC frequency may be caused by an increase in the number of glycinergic synapses, we performed immunostaining of brainstem sections containing the LSO with antibodies specific for GlyT2 or VGAT, synaptic markers for the glycinergic neurons. Consistent with the increased frequency of sIPSCs, we found a significant increase in the intensity of both GlyT2 (Figure 3e-f) and VGAT (Figure 3h-i) staining, suggesting more abundant glycinergic terminals at the LSO of TKO mice. These data together show that the pan-neurexin deletion in MNTB neurons has surprisingly increased the baseline glycinergic neurotransmission likely by promoting the synapse formation/maintenance, which is distinct from the phenotypes observed in glutamatergic and GABAergic neurons (Chen *et al.*, 2017; Luo *et al.*, 2021).

Deletion of neurexins impairs the tight coupling between voltage-gated Ca^{2+} channels and synaptic vesicles at the glycinergic synapse

Because neurexins are shown to exert diverse impacts including specifying the function of voltage-gated Ca^{2+} channels and their spatial clustering within the presynaptic active zone (Chen *et al.*, 2017; Luo *et al.*, 2020; Missler *et al.*, 2003), we addressed these issues by first

exploring the effect of pan-neurexin deletion on the calcium sensitivity of neurotransmitter release at the MNTB-LSO synapse. We perfused the brain slice with low Ca^{2+} (0.2 mM) ACSF while recorded IPSCs continuously. In both control and Nrxn123 TKO mice, the perfusion of low Ca^{2+} ACSF gradually decreased the amplitude of IPSCs (Figure 4a, c). However, the reduction rate was much faster in TKO mice such that IPSC amplitudes dropped more than 50% in TKO vs ~10% in control when extracellular [Ca^{2+}] reached to approximately 1.5 mM (Figure 4b, d). The extracellular [Ca^{2+}] blocking 50% of IPSCs were estimated as 1.1 mM and 1.5 mM respectively for control and TKO mice, which are significantly different (Figure 4e, f), suggesting that neurexins indeed are crucial for regulating calcium sensitivity of transmitter release at the glycinergic synapse.

One of the critical factors affecting the calcium sensitivity of release is the spatial distance between Ca^{2+} channels and synaptic vesicles (Eggermann et al., 2011; Luo *et al.*, 2020). Additionally, neurexins have been shown to promote tight coupling of Ca^{2+} channels with synaptic vesicle at the glutamatergic calyx of Held synapse (Luo *et al.*, 2020). Because the MNTB-LSO glycinergic synapse is similar on multiple aspects of the functional characteristics, being fast, robust, and precise, to the calyx of Held synapse, we tested whether neurexins are also required for the tight coupling of Ca^{2+} channels with synaptic vesicle. We incubated the brain slice with high-concentration EGTA-AM and continuously recorded IPSCs from individual LSO neurons. As illustrated in Figure 5, EGTA-AM treatment slightly blocked IPSCs at control synapses, suggesting the relative ineffectiveness of EGTA in interfering neurotransmitter release (Figure 5a, b). By contrast, at the neurexin-deficient synapses, EGTA-AM treatment remarkably impaired IPSCs (Figure 5c, d). On average, the blocking effects of EGTA at neurexin-deficient synapses (53.2 ± 5.4%) was much stronger than control synapses (15.6 ± 4.3%). Therefore, consistent with previous studies at the calyx of Held synapse (Luo *et al.*, 2020), our data provide further support that neurexins are key synaptic organizers for clustering voltage-gated Ca^{2+} channels tightly with synaptic vesicles at the glycinergic synapse.

Discussion

Using the MNTB-LSO synapse as a model, here we provide first assessment of the role of neurexins at glycinergic synapses that mediate prominent synaptic inhibition in the spinal cord, brainstem and retina. Our findings in general strongly corroborate the idea that neurexins are central presynaptic organizers in all major types of fast chemical synapses including glutamatergic, GABAergic and glycinergic.

Specifically, we have shown that various neurexin genes express concurrently in these glycinergic neurons but the expression level of each appears to vary significantly (Figure 1). This finding is consistent with many studies in glutamatergic and GABAergic neurons, which converge to show that multiple genes, isoforms, and splicing sites of neurexins normally co-express in individual neurons and the expression profiles are highly cell-type specific and brain region specific (Fuccillo *et al.*, 2015; Schreiner et al., 2014; Treutlein et al., 2014; Uchigashima *et al.*, 2019). Distinct neurexins may interact separately and/or redundantly with diverse signaling molecules to form specific molecular codes for shaping neuronal connectivity and functional properties (Aoto et al., 2015; Aoto et al., 2013; Dai et al., 2019; Lin et al., 2023; Lloyd et al., 2023; Sudhof, 2017).

We further show that neurexins are critical in controlling the strength and precise timing of the glycinergic synaptic inhibition at LSO neurons by clustering Ca^{2+} channels tightly with synaptic vesicles in presynaptic release sites (Figures 2, 4 and 5). These data strongly corroborate two perspectives on the function of neurexins as central presynaptic organizers. First, deletion of all neurexins not only weakens the glycinergic synaptic connectivity but also impairs the temporal precision of synaptic inhibition, exactly as it does at the glutamatergic calyx of Held synapse (Luo *et al.*, 2020). Since both the glutamatergic calyx of Held synapse and the glycinergic MNTB-LSO synapse in the auditory brainstem are extremely strong and fast (Beiderbeck et al., 2018; Grothe, 2003), the orchestrating role of neurexins in controlling the timing and magnitude of their synaptic transmission is therefore desirable for the auditory information processing. Secondly, neurexins execute their role at the glycinergic synapse mainly by tightly organizing Ca^{2+} channels within the release sites, again exactly as it does at the calyx of Held synapse (Luo *et al.*, 2020). Nanodomain coupling between Ca^{2+} channels and synaptic vesicles has been found in many fast central synapses and is functionally crucial

for increasing the efficacy and speed of neurotransmission (Eggermann *et al.*, 2011). This similar role of neurexins in clustering Ca^{2+} channels tightly at presynaptic active zones of not only the glutamatergic synapse but also the glycinergic synapse prompts a shared mechanism and further research on the potential molecular candidates.

On the other hand, our data surprisingly reveal that deletion of neurexins may promote the formation/maintenance of the glycinergic synapse, as evidenced by the increase in the frequency of spontaneous synaptic events measured at LSO neurons as well as the increase in the glycinergic synaptic density in Nrxn123 TKO mice (Figure 3). Early studies of TKOs of α-neurexins or β-neurexins lead to general conclusion that neurexins are not essential for the formation/maintenance of excitatory and inhibitory synapses (Anderson *et al.*, 2015; Missler *et al.*, 2003). Moreover, deletion of all α-neurexins and β-neurexins has no impact on the formation/maintenance of glutamatergic synapse (Luo *et al.*, 2020) and GABAergic synapse made by somatostatin-positive interneurons (Chen *et al.*, 2017), but produces partial loss (~30%) of GABAergic synapse made by parvalbumin-positive interneurons (Chen *et al.*, 2017). More recent data even show that Nrxn2 unexpectedly restricts excitatory synapse formation in the hippocampus but has no effect on the inhibitory synapse (Lin *et al.*, 2023). Our present findings on the glycinergic synapse suggest a mix of pro- and anti-synaptogenic effects of neurexins and may raise three possibilities. First, Nrxn2 may dominate its function at this synapse during development and play an inhibitory role in the formation of glycinergic synapse, similar as the previous report of Nrxn2 impact on the hippocampal excitatory synapse (Lin *et al.*, 2023). Second, deletion of neurexins impairs the strength of the MNTB-LSO synapse, which may indirectly interfere with synaptic elimination process and therefore lead to an increase in synaptic density. Third, the more abundant glycinergic synapses may arise from the developmental compensation of synapse formation by other sources of glycinergic neurons (Jalabi *et al.*, 2013). Strong reduction in the strength of the MNTB-LSO synapse caused by selective deletion of neurexins may shift the winner of synaptic competition toward other parallel but much weaker glycinergic inputs in normal animals.

Methods

Mouse breeding and virus injection.

All animal experiments were approved by the Institutional Animal Care and Use Committee at Bioland Laboratory, Guangzhou National Laboratory, Guangzhou, China. Transgenic Nrxn123 cTKO mice of either sex were used for all experiments. Mice were housed at room temperature on a 12 h light–dark cycle (7:00 to 19:00, light) with food and water freely available.

To delete neurexins in MNTB neurons, we injected P0 mice with AAV2/9-hSyn-EGFP-P2A-Cre-WPRE-hGH-Poly (Cat:PT-0156, BrainVTA Co., China). Mice were anesthetized on ice and immediately transferred to a stereotaxic apparatus (RWD Life Technology, China). Injection was achieved by connecting a glass pipette with tip diameter 20-30 μm to Nanoject III programmable nanoliter injector (Drummond Scientific Company, USA). Bilateral injections were performed at the following coordinates: AP from the most rostral point: 5.61 mm, ML: ±0.27 mm, DV: 3.58 mm. For optogenetics experiments, we injected 200 nl (AAV2/9-hSyn-EGFP-P2A-Cre-WPRE-hGH-PolyA and AAV2/9-EF1α-DIO-hChR2(H134R)-mCherry-WPRE-hGH-Poly, 1:1, Cat: PT-0002, BrainVTA Co., China) or 100 nl of AAV2/9-hSyn-hChR2(H123R)-EYFP-WPRE-hGH-PolyA (Cat: PT-1317, BrainVTA Co., China) into each-side MNTB. P13-14 mice of either sex were used for most experiments including electrophysiology, FISH and immunohistochemistry.

Acute slice preparation for electrophysiology

Coronal brain slices containing both the MNTB and LSO were prepared similarly as described previous. In brief, mice of P13-14 were decapitated; brains were rapidly isolated and fixed on the cutting platform a vibratome (VT1200s; Leica, USA), which was immersed in oxygenated cold ACSF containing (in mM): 119 NaCl, 26 $NaHCO_3$, 10 glucose, 1.25 NaH_2PO_4, 2.5 KCl, 0.05 $CaCl_2$, 3 $MgCl_2$, 2 Na-pyruvate, and 0.5 ascorbic acid, pH 7.4. Transverse slices of 250 μm were sectioned and transferred into a beaker with bubbled ACSF containing (in mM): 119 NaCl, 26 NaHCO3, 10 glucose, 1.25 NaH_2PO_4, 2.5 KCl, 2 $CaCl_2$, 1 $MgCl_2$, 2 Na-pyruvate, and 0.5 ascorbic acid, pH 7.4. Slices were recovered at 35°C for 30, and stored at room temperature (~21-23°C) for experiments.

Whole-cell voltage-clamped recordings

Whole-cell voltage-clamped recordings were made from visually identified LSO neurons in acute brain slices using an Axopatch 700B amplifier (Molecular Devices, USA) and pClamp 11 software (Molecular Devices, USA). Patch pipettes were pulled from borosilicate glass capillaries using a two-stage vertical puller (PC-100, Narashige, Japan). Pipette resistance was 4-6 MΩ when filled with an internal solution containing (in mM): 145 K-gluconate, 6 KCl, 10 HEPES, 3 Na_2-phosphocreatine, 4 Mg-ATP, 0.3 Na_2-GTP, 0.2 EGTA, 2 Qx-314; pH 7.2 with KOH. With the extracellular [Cl^-] of 133 mM and a temperature of 22°, the equilibrium potential of the Cl^- was approximately −78.8 mV. In voltage-clamp configuration, IPSCs were recorded by holding cells at 10 mV in ACSF containing CNQX (20 μM), D-AP5 (50 μM), to block AMPA, NMDA receptors, respectively. For some experiments, 2 μM strychnine, a potent glycine receptor antagonist, was added to ACSF to verify that IPSCs recorded at LSO neurons are glycinergic. Membrane potentials were not corrected for liquid junction potential. Electrical fiber stimulation was performed using a concentric bipolar electrode (CBAEB75, FHC Inc, USA) positioned medially to the LSO and MNTB. Short pulses (0.1 ms) were delivered via an isolated stimulator (Model 2100; A-M Systems, USA). For optogenetics, a light simulation of 5 ms was delivered by LED (pE-300 white, CoolLED, UK).

Whole-cell current-clamp recordings

Whole-cell current-clamped recordings were performed similarly as voltage-clamped recordings, except that the internal solution did not contain Qx-314. Action potentials at MNTB neurons were recorded by holding the membrane potential at approximately −70 mV. For optogenetics, a light simulation of 5 ms was delivered by LED (pE-300 white, CoolLED, UK).

RNAscope fluorescent in-situ hybridization (FISH) and immunohistochemistry

Mice were anesthetized and perfused at speed of 1ml/min with 1×PBS for 10 min followed by 4% paraformaldehyde (PFA) for 10 min. Brains were removed and stored in 4% PFA overnight at 4C. After going through a 10%, 20%, and 30% sucrose gradient for cryo-protection, the tissue

was embedded in OCT (Cat：14020108926, Leica) and rapidly frozen on dry ice. Transverse sections at 16 μm were cut at -20 °C using a cryostat (CM3050-S, Leica) and mounted directly on Superfrost Plus slides (Cat: PRO-04, Matsunami Platinum Pro). FISH and immunohistochemistry were performed using the RNAscope multiplex platform (Multiplex Reagent Kit, Cat: 323100; Co-detection ancillary Kit, Cat: 323180, Advanced Cell Diagnostics) following the manufacturer's instructions. RNA probes for Nrxn1, Nrxn2, and Nrxn3 (Cat: 461511-C3, 533531-C2, 505431 respectively, Advanced Cell Diagnostics) and primary antibody against VGluT1 (guinea pig, polyclonal, 1:500, Millipore) were used. Secondary antibodies were Alexa Fluor conjugates (1:400; Thermo Fisher). Samples were mounted with a Vectashield hard-set antifade mounting medium (Cat: H-1500, Vector Laboratories). Images were acquired using Zeiss LSM800 confocal microscopy with a 63x oil-immersion objective (1.4 numerical aperture) or OLYMPUS IXplore SpinSR confocal microscopy with a 60x oil-immersion objective (1.5 numerical aperture). Image analysis were performed using Zeiss 2.6, cellSens Dimension 3.2 and Image J.

Pharmacological manipulations

To estimate the spatial relationship between voltage-gated Ca^{2+} channels and synaptic vesicles, we perfused the slice with ACSF containing 20 μM EGTA-AM for 25~30 mins while continuously recording eIPSC. The blocking effect of EGTA on eIPSCs were evaluated by comparing eIPSCs before and after EGTA treatment.

Statistical analysis

Data were analyzed in the IgorPro (Version 8) and GraphPad Prism 9 software. Summary of data was displayed as mean ± SEM. Statistical analysis was performed using Student's *t* test, two-way ANOVA, and Mann-Whitney U test. Significance of difference was accepted at $P < 0.05$.

References

Anderson, G.R., Aoto, J., Tabuchi, K., Foldy, C., Covy, J., Yee, A.X., Wu, D., Lee, S.J., Chen, L., Malenka, R.C., and Sudhof, T.C. (2015). beta-Neurexins Control Neural Circuits by Regulating Synaptic Endocannabinoid Signaling. Cell *162*, 593-606. 10.1016/j.cell.2015.06.056.

Aoto, J., Foldy, C., Ilcus, S.M., Tabuchi, K., and Sudhof, T.C. (2015). Distinct circuit-dependent functions of presynaptic neurexin-3 at GABAergic and glutamatergic synapses. Nat Neurosci *18*, 997-1007. 10.1038/nn.4037.

Aoto, J., Martinelli, D.C., Malenka, R.C., Tabuchi, K., and Sudhof, T.C. (2013). Presynaptic neurexin-3 alternative splicing trans-synaptically controls postsynaptic AMPA receptor trafficking. Cell *154*, 75-88. 10.1016/j.cell.2013.05.060.

Assareh, N., Fenech, C., Power, R., Uddin, M.N., Otsu, Y., and Aubrey, K.R. (2023). Bidirectional Modulation of Nociception by GlyT2(+) Neurons in the Ventrolateral Periaqueductal Gray. eNeuro *10*. 10.1523/ENEURO.0069-23.2023.

Beiderbeck, B., Myoga, M.H., Muller, N.I.C., Callan, A.R., Friauf, E., Grothe, B., and Pecka, M. (2018). Precisely timed inhibition facilitates action potential firing for spatial coding in the auditory brainstem. Nat Commun *9*, 1771. 10.1038/s41467-018-04210-y.

Boxer, E.E., and Aoto, J. (2022). Neurexins and their ligands at inhibitory synapses. Front Synaptic Neurosci *14*, 1087238. 10.3389/fnsyn.2022.1087238.

Brill, S.E., Maraslioglu, A., Kurz, C., Kramer, F., Fuhr, M.F., Singh, A., and Friauf, E. (2020). Glycinergic Transmission in the Presence and Absence of Functional GlyT2: Lessons From the Auditory Brainstem. Front Synaptic Neurosci *12*, 560008. 10.3389/fnsyn.2020.560008.

Chang, Z., Skach, J., and Kam, K. (2023). Inhibitory subpopulations in preBotzinger Complex play distinct roles in modulating inspiratory rhythm and pattern. bioRxiv. 10.1101/2023.08.07.552303.

Chen, L.Y., Jiang, M., Zhang, B., Gokce, O., and Sudhof, T.C. (2017). Conditional Deletion of All Neurexins Defines Diversity of Essential Synaptic Organizer Functions for Neurexins. Neuron *94*, 611-625 e614. 10.1016/j.neuron.2017.04.011.

Dai, J., Aoto, J., and Sudhof, T.C. (2019). Alternative Splicing of Presynaptic Neurexins Differentially Controls Postsynaptic NMDA and AMPA Receptor Responses. Neuron *102*, 993-1008 e1005. 10.1016/j.neuron.2019.03.032.

Eggermann, E., Bucurenciu, I., Goswami, S.P., and Jonas, P. (2011). Nanodomain coupling between Ca(2)(+) channels and sensors of exocytosis at fast mammalian synapses. Nat Rev Neurosci *13*, 7-21. 10.1038/nrn3125.

Feng, G., Tintrup, H., Kirsch, J., Nichol, M.C., Kuhse, J., Betz, H., and Sanes, J.R. (1998). Dual requirement for gephyrin in glycine receptor clustering and molybdoenzyme activity. Science *282*, 1321-1324. 10.1126/science.282.5392.1321.

Fischer, A.U., Muller, N.I.C., Deller, T., Del Turco, D., Fisch, J.O., Griesemer, D., Kattler, K., Maraslioglu, A., Roemer, V., Xu-Friedman, M.A., et al. (2019). GABA is a modulator, rather than a classical transmitter, in the medial nucleus of the trapezoid body-lateral superior olive sound localization circuit. J Physiol *597*, 2269-2295. 10.1113/JP277566.

Foldy, C., Darmanis, S., Aoto, J., Malenka, R.C., Quake, S.R., and Sudhof, T.C. (2016). Single-cell RNAseq reveals cell adhesion molecule profiles in electrophysiologically defined neurons. Proc Natl Acad Sci U S A *113*, E5222-5231. 10.1073/pnas.1610155113.

Foster, E., Wildner, H., Tudeau, L., Haueter, S., Ralvenius, W.T., Jegen, M., Johannssen, H., Hosli, L., Haenraets, K., Ghanem, A., et al. (2015). Targeted ablation, silencing, and activation

establish glycinergic dorsal horn neurons as key components of a spinal gate for pain and itch. Neuron *85*, 1289-1304. 10.1016/j.neuron.2015.02.028.

Fuccillo, M.V., Foldy, C., Gokce, O., Rothwell, P.E., Sun, G.L., Malenka, R.C., and Sudhof, T.C. (2015). Single-Cell mRNA Profiling Reveals Cell-Type-Specific Expression of Neurexin Isoforms. Neuron *87*, 326-340. 10.1016/j.neuron.2015.06.028.

Gomez, A.M., Traunmuller, L., and Scheiffele, P. (2021). Neurexins: molecular codes for shaping neuronal synapses. Nat Rev Neurosci *22*, 137-151. 10.1038/s41583-020-00415-7.

Gomeza, J., Hulsmann, S., Ohno, K., Eulenburg, V., Szoke, K., Richter, D., and Betz, H. (2003a). Inactivation of the glycine transporter 1 gene discloses vital role of glial glycine uptake in glycinergic inhibition. Neuron *40*, 785-796. 10.1016/s0896-6273(03)00672-x.

Gomeza, J., Ohno, K., Hulsmann, S., Armsen, W., Eulenburg, V., Richter, D.W., Laube, B., and Betz, H. (2003b). Deletion of the mouse glycine transporter 2 results in a hyperekplexia phenotype and postnatal lethality. Neuron *40*, 797-806. 10.1016/s0896-6273(03)00673-1.

Grothe, B. (2003). New roles for synaptic inhibition in sound localization. Nat Rev Neurosci *4*, 540-550. 10.1038/nrn1136.

Grothe, B., Pecka, M., and McAlpine, D. (2010). Mechanisms of sound localization in mammals. Physiol Rev *90*, 983-1012. 10.1152/physrev.00026.2009.

Jalabi, W., Kopp-Scheinpflug, C., Allen, P.D., Schiavon, E., DiGiacomo, R.R., Forsythe, I.D., and Maricich, S.M. (2013). Sound localization ability and glycinergic innervation of the superior olivary complex persist after genetic deletion of the medial nucleus of the trapezoid body. J Neurosci *33*, 15044-15049. 10.1523/JNEUROSCI.2604-13.2013.

Kim, G., and Kandler, K. (2003). Elimination and strengthening of glycinergic/GABAergic connections during tonotopic map formation. Nat Neurosci *6*, 282-290. 10.1038/nn1015.

Kotak, V.C., Korada, S., Schwartz, I.R., and Sanes, D.H. (1998). A developmental shift from GABAergic to glycinergic transmission in the central auditory system. J Neurosci *18*, 4646-4655. 10.1523/JNEUROSCI.18-12-04646.1998.

Krachan, E.G., Fischer, A.U., Franke, J., and Friauf, E. (2017). Synaptic reliability and temporal precision are achieved via high quantal content and effective replenishment: auditory brainstem versus hippocampus. J Physiol *595*, 839-864. 10.1113/JP272799.

Lin, P.Y., Chen, L.Y., Jiang, M., Trotter, J.H., Seigneur, E., and Sudhof, T.C. (2023). Neurexin-2: An inhibitory neurexin that restricts excitatory synapse formation in the hippocampus. Sci Adv *9*, eadd8856. 10.1126/sciadv.add8856.

Lloyd, B.A., Han, Y., Roth, R., Zhang, B., and Aoto, J. (2023). Neurexin-3 subsynaptic densities are spatially distinct from Neurexin-1 and essential for excitatory synapse nanoscale organization in the hippocampus. Nat Commun *14*, 4706. 10.1038/s41467-023-40419-2.

Lukacsovich, D., Winterer, J., Que, L., Luo, W., Lukacsovich, T., and Foldy, C. (2019). Single-Cell RNA-Seq Reveals Developmental Origins and Ontogenetic Stability of Neurexin Alternative Splicing Profiles. Cell Rep *27*, 3752-3759 e3754. 10.1016/j.celrep.2019.05.090.

Luo, F., Sclip, A., Jiang, M., and Sudhof, T.C. (2020). Neurexins cluster Ca(2+) channels within the presynaptic active zone. EMBO J *39*, e103208. 10.15252/embj.2019103208.

Luo, F., Sclip, A., Merrill, S., and Sudhof, T.C. (2021). Neurexins regulate presynaptic GABAB-receptors at central synapses. Nat Commun *12*, 2380. 10.1038/s41467-021-22753-5.

Missler, M., Zhang, W., Rohlmann, A., Kattenstroth, G., Hammer, R.E., Gottmann, K., and Sudhof, T.C. (2003). Alpha-neurexins couple Ca2+ channels to synaptic vesicle exocytosis.

Nature *423*, 939-948. 10.1038/nature01755.
Nabekura, J., Katsurabayashi, S., Kakazu, Y., Shibata, S., Matsubara, A., Jinno, S., Mizoguchi, Y., Sasaki, A., and Ishibashi, H. (2004). Developmental switch from GABA to glycine release in single central synaptic terminals. Nat Neurosci *7*, 17-23. 10.1038/nn1170.
Sanes, D.H., and Friauf, E. (2000). Development and influence of inhibition in the lateral superior olivary nucleus. Hear Res *147*, 46-58. 10.1016/s0378-5955(00)00119-2.
Schreiner, D., Nguyen, T.M., Russo, G., Heber, S., Patrignani, A., Ahrne, E., and Scheiffele, P. (2014). Targeted combinatorial alternative splicing generates brain region-specific repertoires of neurexins. Neuron *84*, 386-398. 10.1016/j.neuron.2014.09.011.
Sudhof, T.C. (2008). Neuroligins and neurexins link synaptic function to cognitive disease. Nature *455*, 903-911. 10.1038/nature07456.
Sudhof, T.C. (2017). Synaptic Neurexin Complexes: A Molecular Code for the Logic of Neural Circuits. Cell *171*, 745-769. 10.1016/j.cell.2017.10.024.
Treutlein, B., Gokce, O., Quake, S.R., and Sudhof, T.C. (2014). Cartography of neurexin alternative splicing mapped by single-molecule long-read mRNA sequencing. Proc Natl Acad Sci U S A *111*, E1291-1299. 10.1073/pnas.1403244111.
Uchigashima, M., Cheung, A., Suh, J., Watanabe, M., and Futai, K. (2019). Differential expression of neurexin genes in the mouse brain. J Comp Neurol *527*, 1940-1965. 10.1002/cne.24664.
Ullrich, B., Ushkaryov, Y.A., and Sudhof, T.C. (1995). Cartography of neurexins: more than 1000 isoforms generated by alternative splicing and expressed in distinct subsets of neurons. Neuron *14*, 497-507. 10.1016/0896-6273(95)90306-2.
Ushkaryov, Y.A., Petrenko, A.G., Geppert, M., and Sudhof, T.C. (1992). Neurexins: synaptic cell surface proteins related to the alpha-latrotoxin receptor and laminin. Science *257*, 50-56. 10.1126/science.1621094.
Zeilhofer, H.U., Wildner, H., and Yevenes, G.E. (2012). Fast synaptic inhibition in spinal sensory processing and pain control. Physiol Rev *92*, 193-235. 10.1152/physrev.00043.2010.

ACKNOWLEDGEMENTS

We thank Dr. B. Zhang (Shenzhen Bay Laboratory) for helpful comments on the manuscript. This study was supported by grants from the National Natural Science Foundation of China (31970914 to F.L.; 32171001, 32371050 to Y.Z.).

AUTHOR CONTRIBUTIONS

Conceptualization, F.L.; Experiments, H.J., R.X., X.N., Z.S., X.X., R. P.; Data analysis, H.J., R.X., X.N., Z.S., X.X., Y.Z, F.L.; Writing – Original Draft, F.L.; Writing – Review & Editing, H.J,

Y.Z, F.L.

DECLARATION OF INTEREST

The authors declare no competing financial interests.

Figure legends

Fig.1 Neurexins are highly expressed in MNTB neurons. (**a**) Immunohistochemistry and RNAscope FISH showing expression of various isoforms of neurexins in the MNTB, which make glycinergic synapses with LSO neurons (**b**) Summary of expression of various isoforms of neurexins in the MNTB of WT mice. (**c**) Diagram of auditory brainstem and virus injection in Nrxn123 cTKO mice. (**d**) Representative images of Nrxn3 FISH in the MNTB of mice injected with AAV-EGFP or AAV-Cre-EGFP. Scale bar: 50 μm. (**e**) Selected ROI in high magnification showing Nrxn3 FISH in MNTB neurons expressing EGFP or Cre-EGFP. Scale bar: 10 μm. (**f**) Summary of expression of various neurexins in the MNTB of Nrxn123 cTKO mice injected with AAV-EGFP and AAV-Cre-EGFP.

Data are means ± SEM. Number of sections analyzed are indicated in the bars (**b**, **f)**; Statistical differences were assessed by Student's t test. (**P < 0.01, ***P < 0.001). Source data are provided as a Source Data file.

Figure 2 Deletion of neurexins reduces the strength and kinetics of glycinergic synapse. (**a**) Representative IPSC traces of LSO neurons evoked by optogenetic stimulation of ChR2 expressed in MNTB neurons. (**b-d**) Summary of IPSC amplitude, rise time, and decay time constant. P = 0.0119, P = 0.0004, P = 0.002. unpaired two-sided t-test. (**e-h**) Same as a-d, except that IPSCs were evoked by afferent fiber stimulation. (**i**) Representative IPSCs traces

of LSO neurons evoked by a pair of fiber stimulation at 50 ms interval. (**j**) Summary of paired-pulse ratio (PPR) of IPSCs in relationship to different paired pulse intervals. P < 0.0001, two-way ANOVA.

Data are means ± SEM. Number of neuron are indicated in the bars (**b-d**, **f-h**) or graph (**j**)**.** Statistical differences were assessed by Student's t test or two-way ANOVA test. (*P < 0.05, **P < 0.01, ***P < 0.001).

Figure 3 Deletion of neurexins increases sIPSC frequency and glycinergic synapse density of LSO neurons. (**a**) Representative sIPSC traces of LSO neurons. (**b**) Summary of sIPSC amplitude and frequency. P = 0.057, P = 0.015, unpaired two-sided t-test. (**c**) Representative sIPSC waveforms of LSO neurons. (**d**) Summary of sIPSC rise time and decay time constant P = 0.376, P = 0.82, unpaired two-sided t-test. (**e**) Representative confocal microscopy images of MNTB-LSO-containing brainstem slice with specific labeling of GlyT2 (red) and EGFP (green) from both control and Nrxn123 TKO mice at P14. Scale bar, 10 µm. (**f**) Summary of GlyT2 immunostaining intensity (normalized to control). P = 2.49E-07, unpaired two-sided t-test. (**g-h**), Same as (**e-f**) except for specific labeling of VGAT (red) and EGFP (green). P = 0.002, unpaired two-sided t-test.

Data are means ± SEM. Number of neuron or sections/animals for immunostaining are indicated in the bars (**b**, **d**, **f** and **h**). Statistical differences were assessed by Student's t test. (*P < 0.05, **P < 0.01, ***P < 0.001). Source data are provided as a Source Data file.

Figure 4 Deletion of neurexins increases the Ca^{2+} sensitivity of release at the glycinergic synapse. (**a**) Representative time courses of IPSC amplitudes for individual LSO neurons of control mice during the perfusion of low Ca^{2+} ACSF. (**b**) Representative IPSC traces of control mice before and during low Ca^{2+} perfusion at the indicated points in **a**. (**c** & **d**) Same as **a** & **b**, except of TKO mice. (**e**) Summary of normalized IPSC amplitudes plotted against the calculated extracellular Ca^{2+} concentration for control and TKO mice. P = 0.0311 for 0.92 mM Ca^{2+}, P = 0.0104 for 1.10 mM Ca^{2+}, P = 0.0208 for 1.28 mM Ca^{2+}, P = 0.0067 for 1.46 mM Ca^{2+}, P = 0.0007 for 1.64 mm Ca^{2+}, unpaired two-sided t-test. (**f**) Summary of IC_{50} of Ca^{2+} for half-blocking of IPSCs and the blocking effect of IPSCs by 0.2 mM Ca^{2+}. P = 0.0139, P

= 0.3985, unpaired two-sided t-test.

Data are means ± SEM. Number of neuron are indicated in the graph (**e**) or bars (**f**). Statistical differences were assessed by Student's t test. (*P < 0.05, **P < 0.01, ***P < 0.001). Source data are provided as a Source Data file.

Figure 5 Deletion of neurexins increases the blocking effect of EGTA on glycinergic IPSCs. (**a**) Representative time courses of IPSC amplitudes for individual LSO neurons of control mice during the treatment of high concentration of EGTA-AM. (**b**) Representative IPSC traces of control mice before and after EGTA. (**c, d**) Same as a, b, except of TKO mice. (**e**) Summary of IPSC amplitude before and after EGTA treatment of control mice. P = 0.0201, paired two-sided t-test. (**f**) Summary of IPSC amplitude before and after EGTA treatment of TKO mice. P = 0.0123, paired two-sided t-test. (**g**) Summary of the blocking percentage of IPSCs by EGTA. P = 0.0001, unpaired two-sided t-test.

Data are means ± SEM. Number of neuron are indicated in the bars (**e** to **g**). Statistical differences were assessed by Student's t test. (*P < 0.05, ***P < 0.001). Source data are provided as a Source Data file.

Figure 1

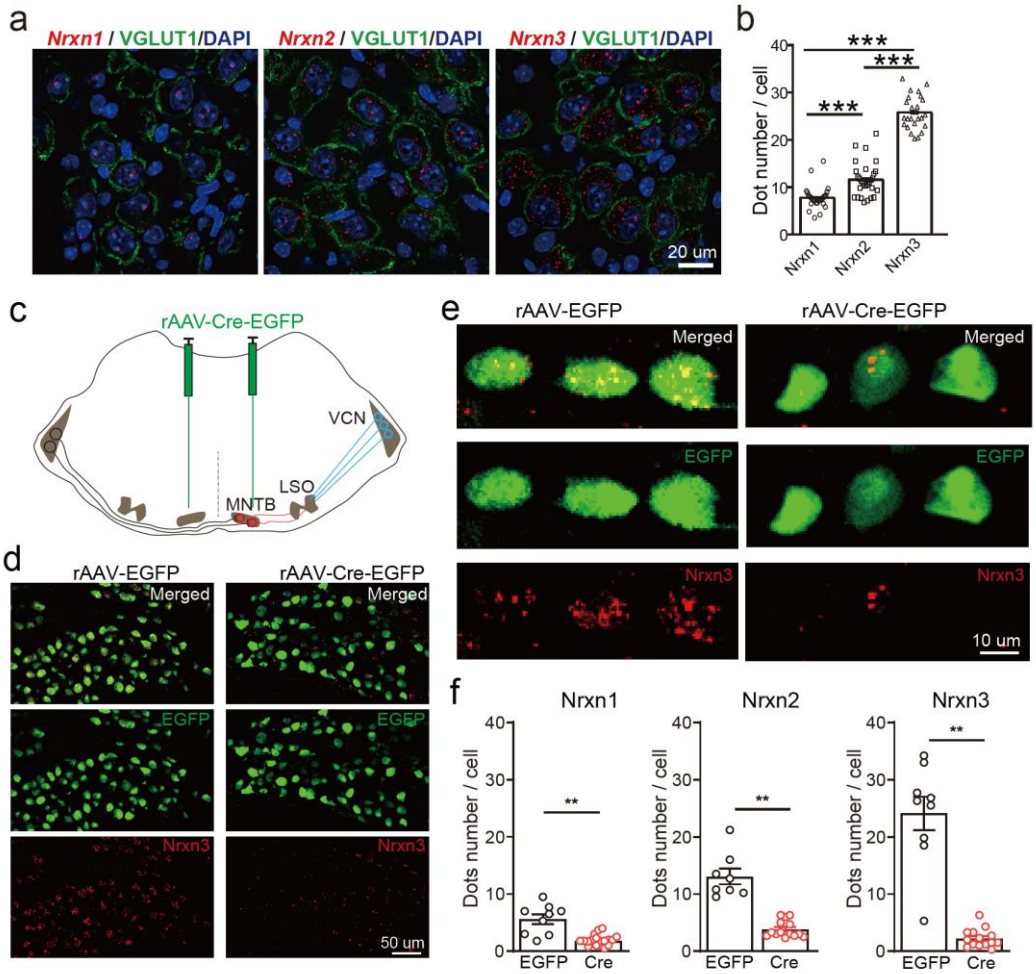
a
Nrxn1 / VGLUT1/DAPI
Nrxn2 / VGLUT1/DAPI
Nrxn3 / VGLUT1/DAPI
20 um
b
Dot number / cell
***
***
***
Nrxn1
Nrxn2
Nrxn3
c
rAAV-Cre-EGFP
VCN
LSO
MNTB
d
rAAV-EGFP
rAAV-Cre-EGFP
Merged
EGFP
Nrxn3
50 um
e
rAAV-EGFP
rAAV-Cre-EGFP
Merged
EGFP
Nrxn3
10 um
f
Nrxn1
Nrxn2
Nrxn3
Dots number / cell
**
EGFP
Cre

Figure 2

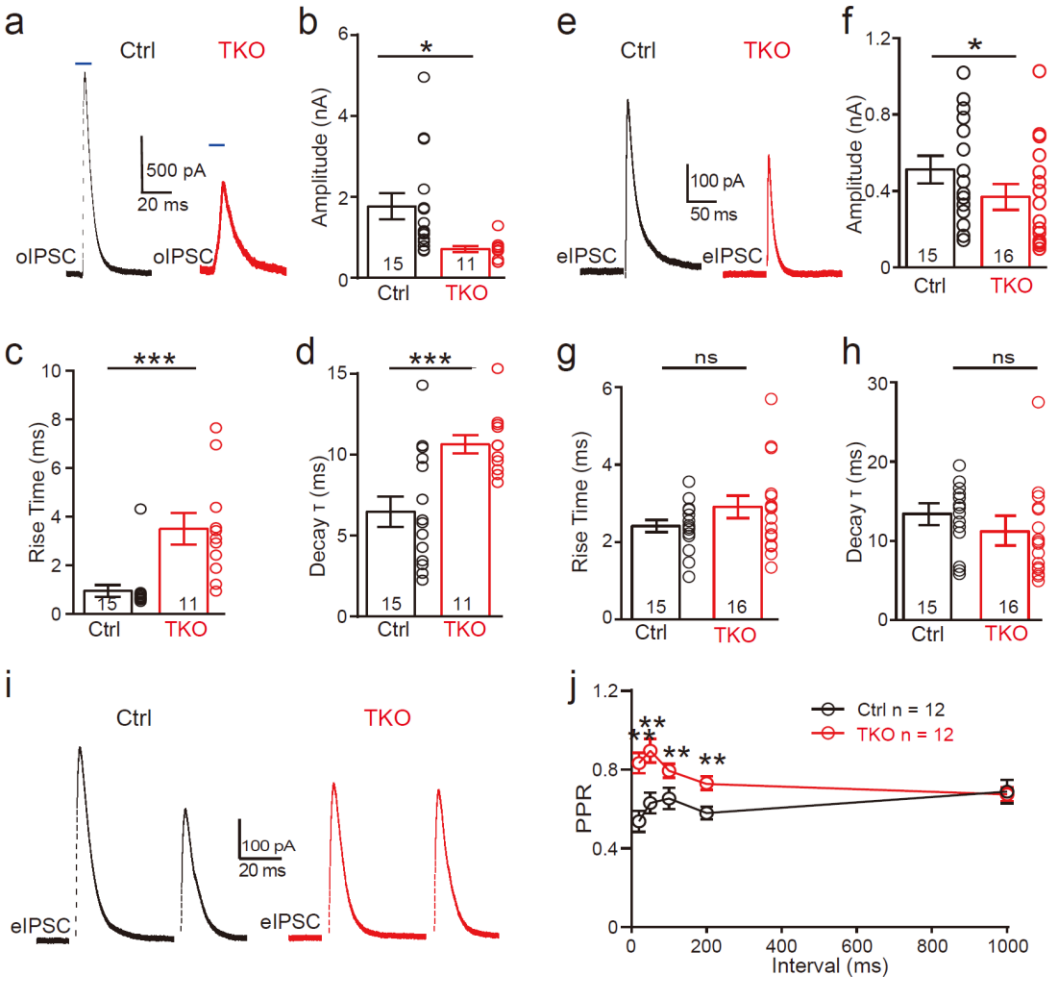
a
Ctrl
TKO
500 pA
20 ms
oIPSC
oIPSC
b
Amplitude (nA)
*
15
11
Ctrl
TKO
e
Ctrl
TKO
100 pA
50 ms
eIPSC
eIPSC
f
Amplitude (nA)
*
15
16
Ctrl
TKO
c
Rise Time (ms)
***
15
11
Ctrl
TKO
d
Decay τ (ms)
***
15
11
Ctrl
TKO
g
Rise Time (ms)
ns
15
16
Ctrl
TKO
h
Decay τ (ms)
ns
15
16
Ctrl
TKO
i
Ctrl
TKO
100 pA
20 ms
eIPSC
eIPSC
j
PPR
Ctrl n = 12
TKO n = 12
**
**
**
**
Interval (ms)

561 **Figure 3**

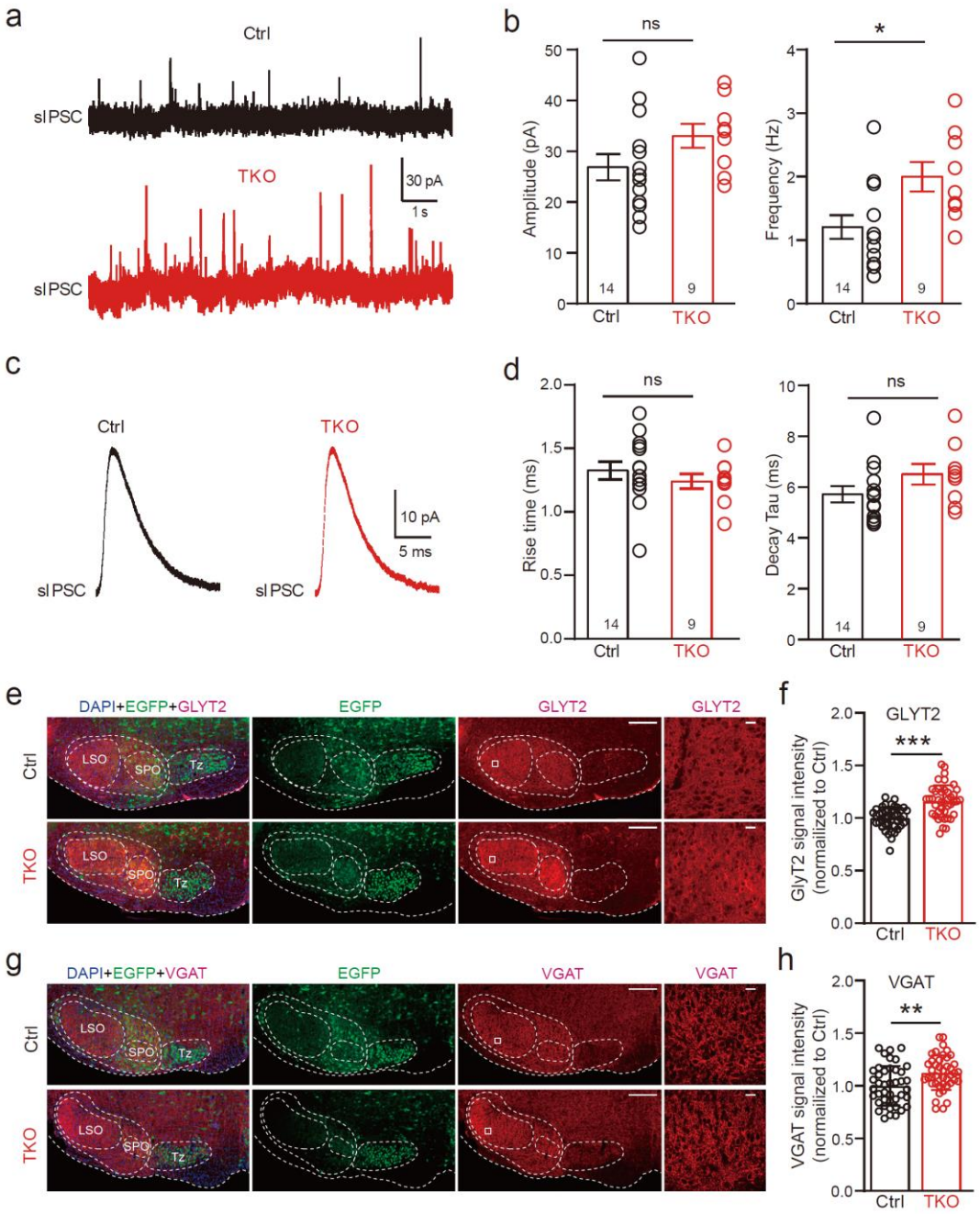

562

563

Figure 4

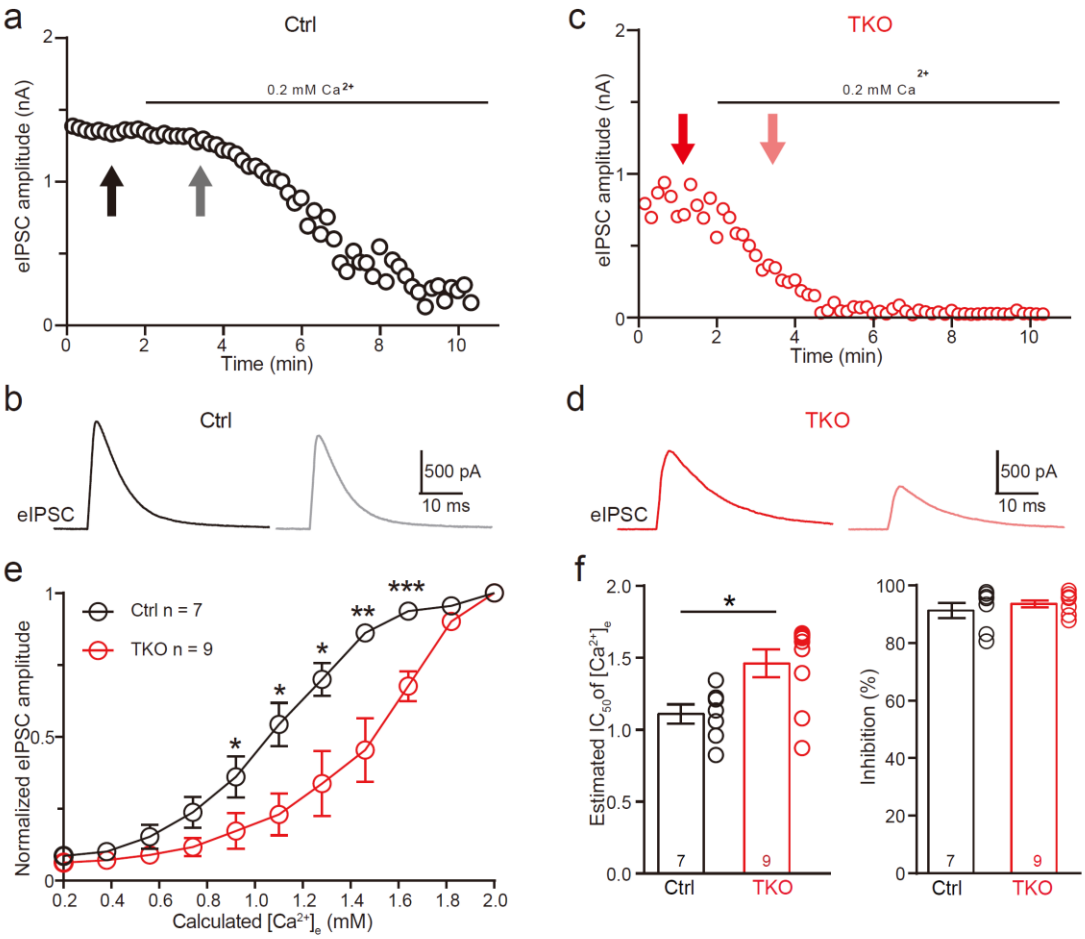
a
Ctrl
0.2 mM Ca2+
eIPSC amplitude (nA)
Time (min)
c
TKO
0.2 mM Ca2+
eIPSC amplitude (nA)
Time (min)
b
Ctrl
eIPSC
500 pA
10 ms
d
TKO
eIPSC
500 pA
10 ms
e
Ctrl n = 7
TKO n = 9
Normalized eIPSC amplitude
Calculated [Ca2+]e (mM)
f
Estimated IC50 of [Ca2+]e
Ctrl
TKO
Inhibition (%)
Ctrl
TKO

Figure 5

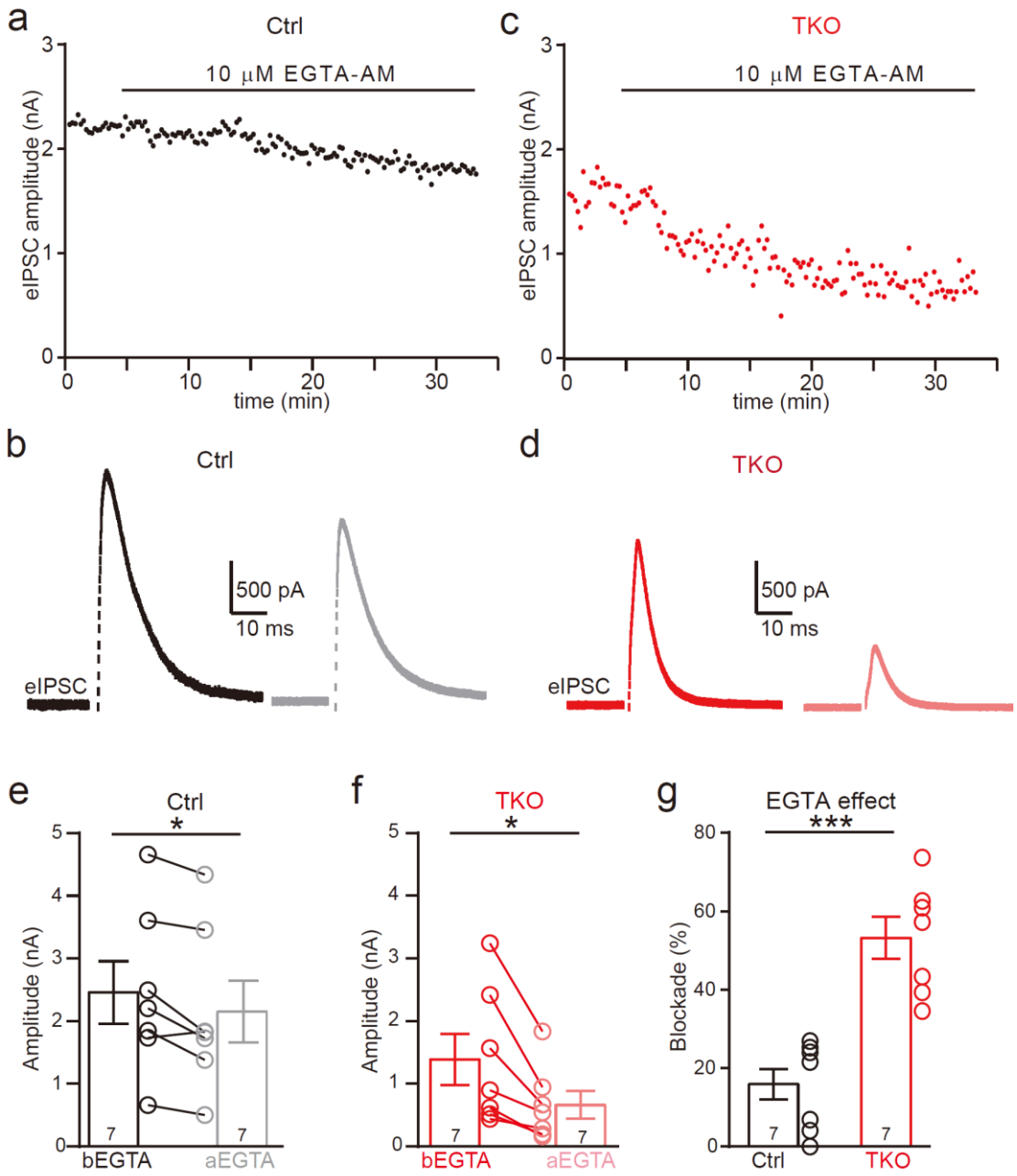
a
Ctrl
10 μM EGTA-AM
eIPSC amplitude (nA)
time (min)
c
TKO
10 μM EGTA-AM
eIPSC amplitude (nA)
time (min)
b
Ctrl
500 pA
10 ms
eIPSC
d
TKO
500 pA
10 ms
eIPSC
e
Ctrl
*
Amplitude (nA)
bEGTA
aEGTA
f
TKO
*
Amplitude (nA)
bEGTA
aEGTA
g
EGTA effect
***
Blockade (%)
Ctrl
TKO

Figure S1

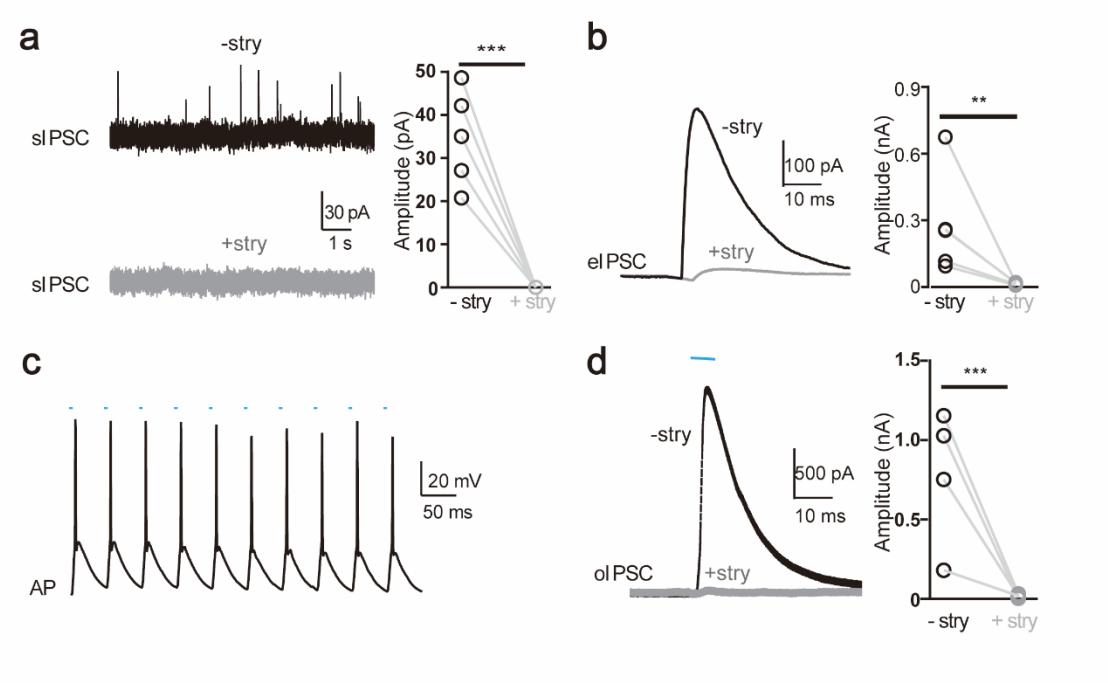

a Representative sIPSC traces of LSO neurons before and after application of potent glycine receptor blocker strychine (stry) (left) and summary of sIPSC amplitude without and with stry (right).
b Representative eIPSC traces of LSO neurons before and after stry application (left) and summary of eIPSC amplitude without and with stry (right).
c Representative action potential (AP) firing of MNTB neurons infected with ChR2 during high frequency repetitive pulse stimulation of 473 nm.
d Representative oIPSC traces of LSO neurons before and after stry application (left) and summary of oIPSC amplitude without and with stry (right).

Figure s2

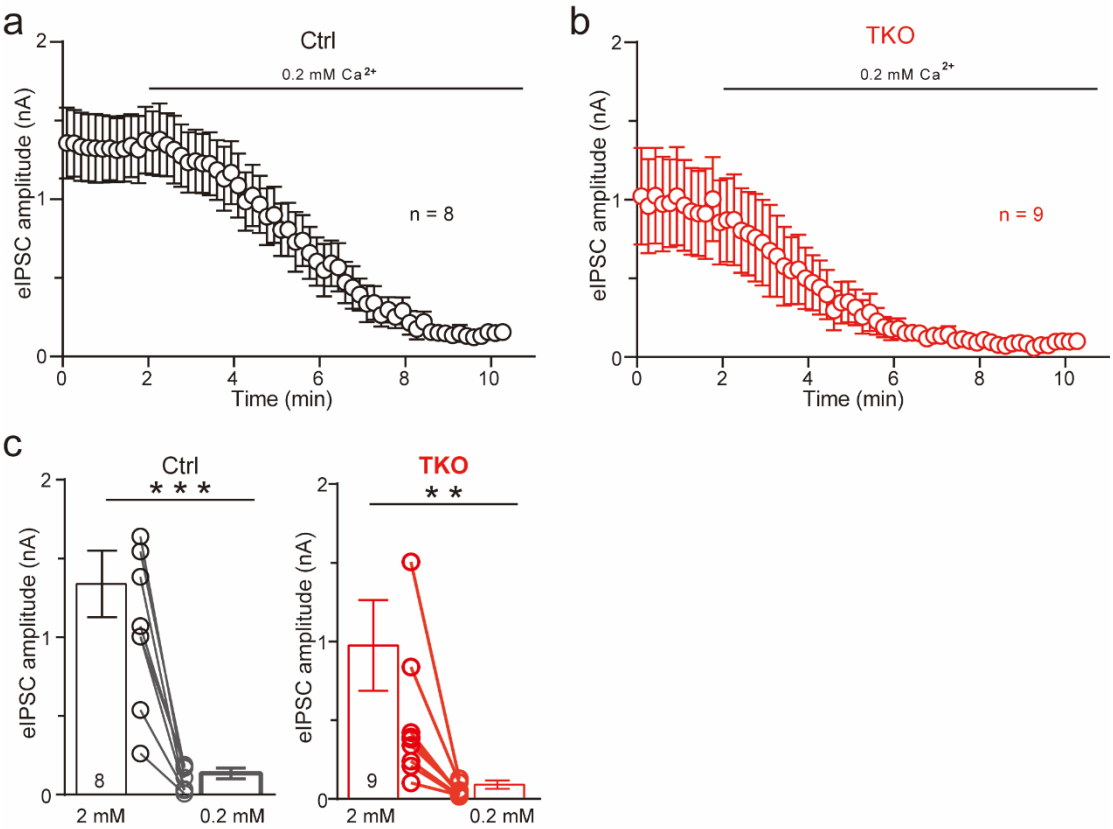

a Summary of eIPSC amplitude of control during 0.2 mM Ca^{2+} perfusion. Mean ± SEM.
b Summery of eIPSC amplitude of TKO during 0.2 mM Ca^{2+} perfusion. Mean ± SEM.
c Average of eIPSC amplitude before and after 0.2 mM Ca^{2+} perfusion. Mean ± SEM.
(**P < 0.01, ***P < 0.001), paired t-test.

Figure s3

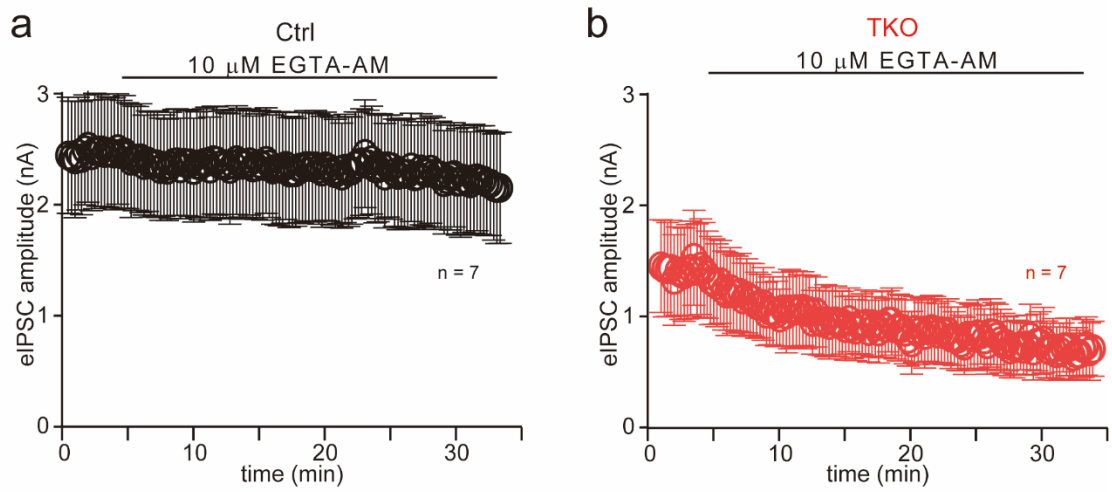

a Summary of eIPSC amplitude of control during 10 μM EGTA-AM treatment. Mean ± SEM.
b Summary of eIPSC amplitude of TKO during 10 μM EGTA-AM treatment. Mean ± SEM